Semi-Analytical Finite-Element Study for Elastomeric Composite Solids of Revolution

Moetaz M. El-Hawary* and Leonard R. Herrmann†
University of California, Davis, Davis, California

The research presented in this paper is concerned with the development of a linear composite theory, along with a semi-analytical finite-element analysis for horizontally layered, reinforced, elastomeric bearings of revolution subjected to nonaxisymmetric loads. A multiscale representation is used in the development of the composite theory to model both small and large-scale stress and deformation phenomena. In addition to the usual displacement variables, special field variables are introduced to model "edge effect" phenomena. In contrast to some previous work, only continuity of the field variables (but not their derivatives) is required for the resulting finite-element analysis, thus permitting use of simple bilinear four-node isoparametric elements. Several numerical examples are presented and compared to discrete and previously obtained composite analyses. A section is devoted to the comparison of the present results to available design curves for elastomeric bearings used in helicopter systems. For the purpose of illustrating the general capabilities of the theory and analysis, a parameter study for a class of horizontal layered elastomeric bearings with a conical central hole is performed; the effects of varying the angle between the inner surface of the bearing and the vertical axis are evaluated under different loading conditions.

Introduction

ELASTOMERIC bearings consist of alternate layers of stiff and flexible materials (examples of common constituent materials are steel and rubber, and fiberglass and rubber). They are used for a wide range of applications, including building isolations pads for seismic or noise control,[1] flex seals for rocket engines,[2] rotor head bearings for helicopters,[3] and bearing pads for bridges.[4,5]

Because of the large number of component layers, these composite systems are geometrically complex; however, the development of the finite-element method and the use of high-speed computers have, in theory, made it possible to model such geometric details. The modeling of such complex systems, however, often requires excessive computer time, especially in cases where three-dimensional, dynamic, nonlinear and/or inelastic effects must be included. The main focus of this paper is the development of an alternative efficient finite-element analysis of such systems.

The special class of layered systems considered in this work consist of horizontally layered solids of revolution, i.e., the geometry of the bearing is symmetric about an axis of revolution. Perfect bonding between the flexible pads and the stiff shims, small deformations and deflections, and linear elastic material behavior are assumed.

Two general finite-element approaches to the analysis of layered systems are used in practice, namely, discrete and composite.[6-9] In a discrete analysis, the bearing is analyzed as a heterogeneous body where each element contains only one type of material; thus, material interfaces fall along element boundaries. A discrete model usually requires a very fine mesh; thus, the computational cost of the analysis can be excessive. The advantage of the discrete method is that local stresses and strains are directly obtained.

In a composite model, the homogeneous continuum concept is extended to include layered systems. The continuum concept models the system as an equivalent orthotropic, homogeneous material. This concept has been used for years in modeling composite materials such as concrete, and relatively recently it has been applied to many structural composites. In a composite analysis, each element may contain more than one type or layer of material, which permits the use of a much coarser mesh (to render the same accuracy) than is possible for a discrete analysis. The advantage of using a composite analysis is the economy achieved in using a coarse mesh. The main disadvantage is that interface stresses and strains are not directly obtained. Also, edge-effect parameters must be included in the composite analysis to model localized effects near the boundaries of the system.

Edge effects arise at boundaries of composites due to the material property discontinuities. For many composites such as concrete,[10] they are of little consequence; however, for other systems (particularly layered systems composed of materials with dramatically different shear stiffnesses), they are of fundamental importance.[6-8] Various procedures have been used by researchers to develop economically feasible analyses for composites that are capable of including edge effects and of obtaining local stresses with acceptable accuracy. These methods include discrete analyses with substructuring in critical regions,[11] the adding (to form a composite stiffness matrix) of the stiffness matrices of the constituent layers (and of fictitious links along their interfaces[7]) that occupy the domain of the composite element, the formal application of the mathematical methods of perturbation,[6,12] the introduction of higher-order continuum theories that are capable of modeling the material's microsubstructure,[13,14] the use of a composite theory that is derived by superimposing fundamental deformation modes,[8,15] and, finally, the use of multi-scale expansions for displacement approximation that are then used in approximating the strain energy of the system.[16-18]

When a theory that includes edge effects is developed by the superposition of fundamental deformation modes,[8,15] the direct extension of the theory to include the modeling of

Received May 26, 1987; revision received Dec. 14, 1987.

*Post Doctorate Research Engineer.
†Professor of Civil Engineering, Division of Aeronautical Science and Engineering.

nonlinear behavior is not possible. In contrast, the multiple spatial scales theory[16–18] has the ability to include both edge and nonlinear effects; this approach will be used in the present work and will be explained more fully later.

In finite-element applications, three-dimensional problems are avoided when possible because of the very considerable increase of conputational cost as compared to two-dimensional problems. Semi-analytical finite-element methods used Fourier series representations in one direction and standard finite-element approximations in the other two. For linear problems, the semi-analytical method leads to uncoupled sets of simultaneous equations, thus considerably reducing the cost of the overall solution when compared to a standard three-dimensional finite-element analysis.

Semi-analytical methods have been used for linear problems involving solids of revolution[19,20] and infinite prismatic solids.[21] Attempts have been made to lift some of the restrictions on the use of the semi-analytical method for nonlinear problems.[22] In the present work, a semi-analytical finite-element procedure is used to analyze nonaxisymmetrically loaded, horizontally laminated, elastomeric bearings of revolution.

Theory

The theory is an extension of the two-dimensional composite theory for the axisymmetric loading of layered solids of revolution developed by El-Hawary.[18] The theory will be limited to bearings with horizontal layers; however, the concepts can be extended to other axisymmetric configurations.

The concepts of multiple spatial scales and edge-effect variables as introduced by Lim[16] are used in the present theory, and it is assumed that the reader is familiar with these concepts. It is sufficient to note here that the introduction of multiple spatial scales [23] permits the simultaneous description of physical phenomena for whom the rapidity of variations in space are radically different (e.g., edge effects and interior behavior).

Field Variables

The primary displacement variables selected for the composite theory consist of the centerline displacements u, v, and w of the stiff layers, the rotations ϕ_r and ϕ_θ of the "normal fiber" for the stiff layers, and the averaging bulging δ_r and δ_θ of the flexible layers relative to the stiff layers. It is to be noted that the flexible layer "bulging" is, in general, an edge-effect phenomenon. The stiff layer centerline displacements u, v, and w and the rotations ϕ_r and ϕ_θ are, in reality, only defined and have physical meaning at the centers of the stiff layers. However, in the composite theory (locations of individual layers are not precisely defined), they are treated as continuous field variables.

The rationale for the selection of this set of variables is given by Lim,[16] their meanings will be clarified in the subsequent derivations. For illustration of some of these quantities, the reader is referred to Fig. 1 where the stiff-layer kinematics are shown in three views: u, v, and w are the displacement components of the centerline of the stiff layer in the r, θ, and z directions, respectively, and ϕ_r and ϕ_θ are the rotations of the normal fiber about the θ and r axes (the superscript * will be explained later).

In addition to the above listed variables, for the sake of reducing the complexity of the energy expression, three expansion variables D_1, D_2, and D_3 that relate to the thickness deformation of the flexible layers are retained in the analysis to the point of forming the element stiffness matrices, at which time they are eliminated by "element condensation."[24]

Fourier Series Representation

The field variables are expanded in Fourier series, e.g.,

$$u = \sum_{m_1=0}^{M_1} u_{m_1} \cos(m_1\theta) + \sum_{m_2=1}^{M_2} u_{m_2} \sin(m_2\theta), \text{ etc.} \qquad (1)$$

To simplify these equations, the notation introduced by Sedaghat[22] is used, i.e.,

$$T_m(\theta) = \begin{cases} \cos(|m|\theta) & \text{when } m \geq 0 \\ \sin(|m|\theta) & \text{when } m < 0 \end{cases} \qquad (2)$$

$$\frac{dT_m}{d\theta} = -mT_{-m} \qquad (3)$$

Introducing the above into Eq. (1) gives:

$$u = \sum_{m=-M_2}^{M_1} u_m T_m = u_m T_m \qquad (4)$$

where summation is implied over repeated indices (note in the series for v, ϕ_θ, and δ_θ, T_m is replaced by T_{-m}).

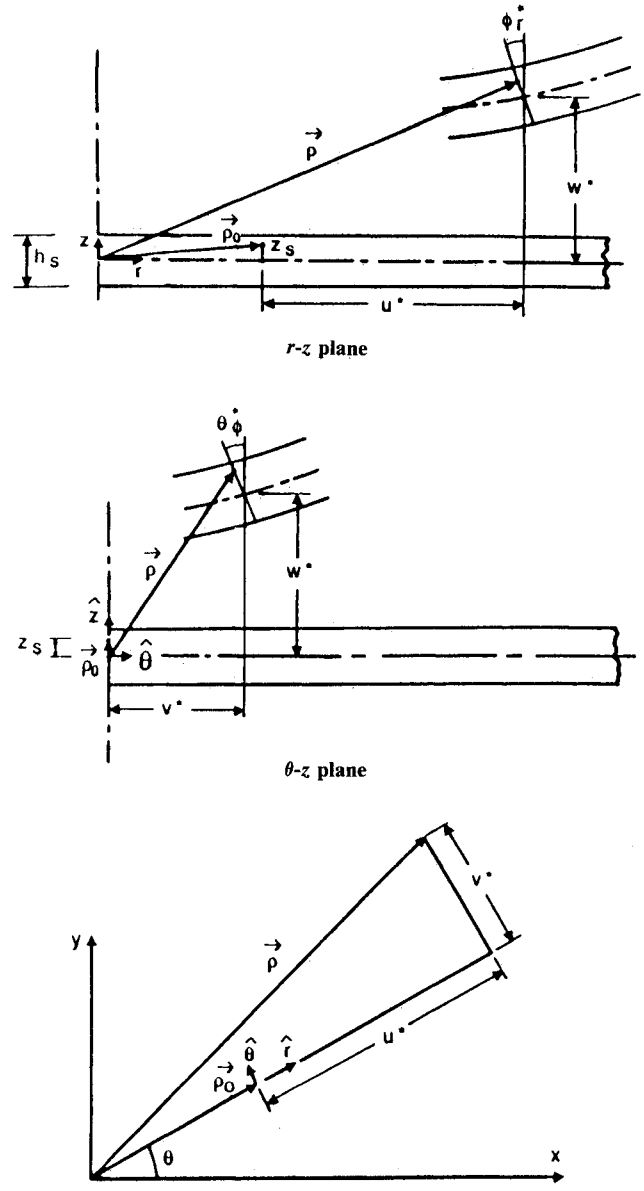

Fig. 1 Stiff-layer kinematics.

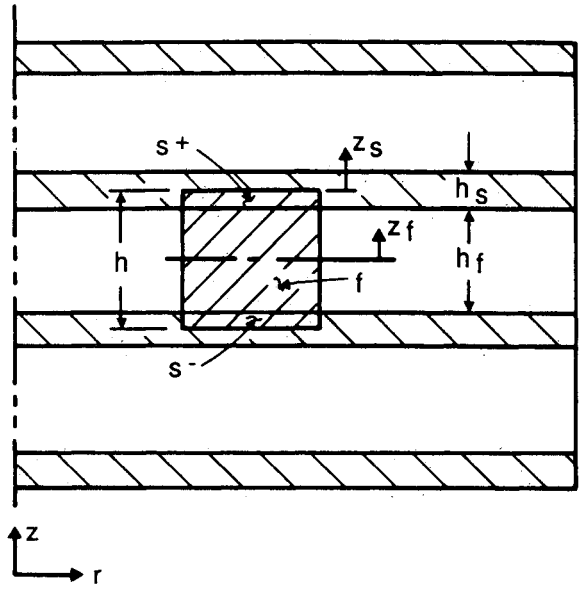

Fig. 2 Portion of an elastomeric bearing illustrating the unit cell.

Stiff-Layer Kinematics

The stiff-layer deformation is shown in Fig. 1. The initial position vector is

$$\rho_0 = r\,\hat{r} + \frac{h_s z_s}{2}\hat{z} \tag{5}$$

and assuming small deflections, the final position vector is

$$\rho = [r + u^* - (h_s z_s/2)\phi_r^*]\,\hat{r} + [v^* - (h_s z_s/2) + \phi_\theta^*]\hat{\theta} + [w_1^* + (h_s z_s/2) + w^*]\hat{z} \tag{6}$$

where z_s is the local vertical coordinate for the stiff layers, and $\hat{r}$, $\hat{\theta}$, and $\hat{z}$ are the unit vectors in the r, θ, and z directions, respectively. The deflection due to the change in thickness of a stiff layer is written as w_1^*. The superscript * is used to indicate the value of a quantity evaluated at the center of a stiff layer (hence, independent of z_s and z). (More precisely, the quantities u^*, v^*, etc., are parameters that define the approximations used for the local displacement fields in the unit cell. It is their identification with the values of the global field variables u, v, etc., at the center of the layer that approximately establishes continuity of deformation between adjacent unit cells, (see Ref. 16).

Substracting ρ_0 from ρ gives the displacement vector; substituting its components into the strain displacement equations and neglecting the derivatives of w_1^* when compared to those of w^* gives

$$\epsilon_{r_s} = u^*_{,r} - \phi^*_{r,r}\,(h_s z_s/2) \tag{7}$$

$$\epsilon_{\theta_s} = (1/r)\,[u^* + v^*_{,\theta} - (h_s z_s/2)\phi_r^* - (h_s z_s/2)\phi^*_{\theta,\theta}] \tag{8}$$

$$\gamma_{rz_s} = -\phi_r^* + w^*_{,r} \tag{9}$$

$$\gamma_{\theta r_s} = (1/r)\,[u^*_{,\theta} - v^* + r v^*_{,r} - (h_s z_s/2)(\phi^*_{r,\theta} + r\phi^*_{\theta,r} - \phi^*_\theta)] \tag{10}$$

$$\gamma_{\theta z_s} = (1/r)\,w^*_{,\theta} - \phi^*_\theta \tag{11}$$

$$\epsilon_{z_s} = (2/h_s)\,w^*_{1,z_s} \tag{12}$$

Recognizing the fact that the strain in the z direction is mainly due to Poisson's effect plus a small amount D_1^* due to the normal stress yields ($\alpha_i = \nu_i/(1-\nu_i)$ where Poisson's ratio is denoted by ν):

$$\epsilon_{z_s} = -\alpha_s[u^*_{,r} - \phi^*_{r,r}(h_s z_s/2) + (u^*/r) + (v^*_{,\theta}/r) - (h_s z_s/2r)\,\phi_r^* - (h_s z_s/2r)\,\phi^*_{\theta,\theta}] + D_1^* \tag{13}$$

Equating Eqs. (12) and (13), solving for w^*_{1,z_s}, integrating and neglecting the bending terms since they do not contribute to the overall change in thickness, gives

$$w_1^* = (h_s/2)\{D_1^* - \alpha_s\,[u^*_{,r} + (u^*/r) + (v^*_{,\theta}/r)]\}z_s \tag{14}$$

Introducing the Fourier series representation gives

$$\epsilon_{r_s} = [u^*_{m,r} - \phi^*_{r_{m,r}}(h_s z_s/2)]T_m, \text{ etc.} \tag{15}$$

Compatibility Conditions

As noted above, the displacement components are obtained from ρ and ρ_0; their Fourier components are

$$u_{s_m} = u_m^* - (h_s z_s/2)\phi^*_{r_m} \tag{16}$$

$$v_{s_m} = v_m^* - (h_s z_s/2)\phi^*_{\theta_m} \tag{17}$$

$$w_{s_m} = w_m^* + w^*_{1_m} \tag{18}$$

The field variables are approximated in terms of truncated Taylor series about the center of the unit cell, which is the smallest representative building block of the system (see Fig. 2). Denoting the upper stiff layer in the unit cell by $+$, the lower one by $-$, and the evaluation of the function at the center of the unit cell by**, the Fourier coefficients of the field variables evaluated at the center of the two stiff layers are ($h = h_s + h_f$):

$$u_m^* = u^{**}_m \pm (h/2)u^{**}_{m,z}, \text{ etc.} \tag{19}$$

Using the above expression [also using Eq. (14) and neglecting the small quantity $w^{**}_{1,z}$] to eliminate the * quantities from Eqs. (16–18) gives

$$u^{\pm}_{s_m} = u^{**}_m \pm (h/2)u^{**}_{m,z} - (h_s/2)(\phi^{**}_{r_m} \pm (h/2)\phi^{**}_{r_{m,z}})z_s \tag{20}$$

$$v^{\pm}_{s_m} = v^{**}_m \pm (h/2)v^{**}_{m,z} - (h_s/2)(\phi^{**}_{\theta_m} \pm (h/2)\phi^{**}_{\theta_{m,z}})z_s \tag{21}$$

$$w^{\pm}_{s_m} = w^{**}_m \pm (h/2)w^{**}_{m,z} + (h_s/2) \times \left[D^{**}_{1_m} - \alpha_s\left(u^{**}_{m,r} + \frac{u^{**}_m}{r} - m\frac{v^{**}_m}{r}\right)\right]z_s \tag{22}$$

The displacement components u_f, v_f, and w_f for the flexible layer are also expanded in terms of Fourier series:

$$u_f = u_{f_m}T_m, \text{ etc.} \tag{23}$$

Guided by Lim's work,[16] the following variations for the flexible layer displacement components across the thickness of the layer are assumed:

$$u_{f_m} = u^{**}_m + C^{**}_{0_m} + C^{**}_{1_m}z_f + 3(\delta^{**}_{r_m} - C^{**}_{0_m})\,z_f^2 \tag{24}$$

$$v_{f_m} = v^{**}_m + E^{**}_{0_m} + E^{**}_{1_m}z_f + 3(\delta^{**}_{\theta_m} - E^{**}_{0_m})\,z_f^2 \tag{25}$$

$$w_{f_m} = w^{**}_m + D^{**}_{0_m} + D^{**}_{1_m}z_f + D^{**}_{2_m}\,z_f^2 + D^{**}_{3_m}\,z_f^3 \tag{26}$$

The first terms in the above expressions can be viewed as values obtained by interpolating the displacements of the neighboring stiff layers, and then the remaining terms can be viewed as corrections to account for displacement of the flexible material relative to the stiff layers. The forms of the

correction terms can be either interpreted as truncated power series expansions, or the physical arguments given by Lim[16] can be invoked to arrive at the expressions in question.

Interface compatibility between the layers is satisfied for each individual Fourier term by requiring that the displacement components of the stiff and flexible materials be equal at their interface, e.g.,

$$u_{f_m}\Big|_{\pm 1} = u_{s_m}^{\pm}\Big|_{\mp 1}, \text{ etc.} \tag{27}$$

These conditions give relations of the form

$$C_{0_m}^{**} = (3/2)\delta_{r_m}^{**} - (h\,h_s/8)\phi_{r_{m,z}}^{**}, \text{ etc.} \tag{28}$$

Substituting back into Eqs. (24–26), the displacement components for a point in a flexible layer for the mth Fourier term are

$$u_{f_m} = u_m^{**} + \frac{3}{2}\delta_{r_m}^{**} - \frac{h\,h_s}{8}\phi_{r_{m,z}}^{**} + \left(\frac{h}{2}u_{m,z}^{**} + \frac{h_s}{2}\phi_{r_m}^{**}\right) z_f + 3\left(-\frac{\delta_{r_m}^{**}}{2} + \frac{h\,h_s}{8}\phi_{r_{m,z}}^{**}\right) z_f^2 \tag{29}$$

$$v_{f_m} = v_m^{**} + \frac{3}{2}\delta_{\theta_m}^{**} - \frac{h\,h_s}{8}\phi_{\theta_{m,z}}^{**} + \left(\frac{h}{2}v_{m,z}^{**} + \frac{h_s}{2}\phi_{\theta_m}^{**}\right) z_f + 3\left(-\frac{\delta_{\theta_m}^{**}}{2} + \frac{h\,h_s}{8}\phi_{\theta_{m,z}}^{**}\right) z_f^2 \tag{30}$$

$$w_{f_m} = w_m^{**} - D_{2_m}^{**} + \left\{-D_{3_m}^{**} + \frac{h}{2}w_{m,z}^{**} + \frac{h_s}{2}\left[\alpha_s\left(u_{m,r}^{**} + \frac{u_m^{**}}{r} + m\frac{v_m^{**}}{r}\right) - D_{1_m}^{**}\right]\right\} z_f + D_{2_m}^{**} z_f^2 + D_{3_m}^{**} z_f^3 \tag{31}$$

Flexible-Layer Kinematics

In the following consideration of strains, several approximations will be made. In the spirit of the Taylor series approximation used in Eq. (19) for the z dependence of a function, second derivatives in r are neglected;[16] accordingly, derivatives of the quantities D_i are neglected, since the D_i were shown by Lim[16] to be functions of the first derivatives of the field variables. The term in Eq. (31) resulting from Poisson's effect due to the in-plane stretching of the stiff layers is neglected in the calculation of γ_{rz_f} and $\gamma_{r\theta_f}$. Substituting the displacements into the strain-displacement equations in cylindrical coordinates, and defining $\rho = h_s/h_f$, leads to

$$\epsilon_{r_f} = \left[u_{m,r}^{**} + \frac{h_s}{2}\phi_{r_{m,r}}^{**} z_f + \frac{3}{2}(1 - z_f^2)\,\delta_{r_{m,r}}^{**}\right] T_m \tag{32}$$

$$\epsilon_{z_f} = \left[(1+\rho)\,w_{m,z}^{**} - \frac{2}{h_f}D_{3_m}^{**} + \rho\,\alpha_s\left(u_{m,r}^{**} + \frac{u_m^{**}}{r} + m\frac{v_m^{**}}{r}\right) - \rho\,D_{1_m}^{**} + \frac{4}{h_f}D_{2_m}^{**} z_f + \frac{6}{h_f}D_{3_m}^{**} z_f^2\right] T_m \tag{33}$$

$$\epsilon_{\theta_f} = \left\{\frac{1}{r}\left[m\,v_m^{**} + \frac{h_s}{2}m\,\phi_{\theta_m}^{**} z_f + \frac{3}{2}(1 - z_f^2)\,m\,\delta_{\theta_m}^{**} + u_m^{**} + \frac{3}{2}(1 - z_f^2)\,\delta_{r_m}^{**} + \frac{h\,h_s}{8}(3\,z_f^2 - 1) \times \phi_{r_{m,z}}^{**} + \left(\frac{h}{2}u_{m,z}^{**} + \frac{h_s}{2}\phi_{r_m}^{**}\right) z_f + \frac{h}{2}m\,v_{m,z}^{**} z_f + \frac{h\,h_s}{8}m\,\phi_{\theta_{m,z}}^{**}(3\,z_f^2 - 1)\right]\right\} T_m \tag{34}$$

$$\gamma_{rz_f} = \left[(1+\rho)\,u_{m,z}^{**} + \rho\phi_{r_m}^{**} - \frac{6}{h_f}z_f\delta_{r_m}^{**} + \frac{3}{2}h_s(1+\rho)\,z_f\,\phi_{r_{m,z}}^{**} + w_{m,r}^{**}\right] T_m \tag{35}$$

$$\gamma_{r\theta_f} = \left\{-m\frac{u_m^{**}}{r} - \frac{3}{2r}(1 - z_f^2)m\,\delta_{r_m}^{**} - \frac{h_s}{2r}m\,z_f\,\phi_{r_m}^{**} + v_{m,r}^{**} + \frac{3}{2}(1 - z_f^2)\,\delta_{\theta_{m,r}}^{**} + \frac{h_s}{2}z_f\,\phi_{\theta_{m,r}}^{**} - \frac{1}{r} \times \left[v_m^{**} + \frac{3}{2}\delta_{\theta_m}^{**} - \frac{h\,h_s}{8}\phi_{\theta_{m,z}}^{**} + \left(\frac{h}{2}v_{m,z}^{**} + \frac{h_s}{2}\phi_{\theta_m}^{**}\right) z_f + 3\left(-\frac{\delta_{\theta_m}}{2} + \frac{h\,h_s}{8}\phi_{\theta_{m,z}}^{**}\right) z_f^2 + \frac{h}{2}m\,z_f\,u_{m,z}^{**} + \frac{h\,h_s}{8}m\,\phi_{r_{m,z}}^{**}(3\,z_f^2 - 1)\right]\right\} T_{-m} \tag{36}$$

$$\gamma_{\theta z_f} = \left\{(1+\rho)\,v_{m,z}^{**} + \rho\,\phi_{\theta_m}^{**} - \frac{6}{h_f}z_f\,\delta_{\theta_m}^{**} + \frac{3}{2}h_s\,(1+\rho) \times z_f\,\phi_{\theta_{m,z}}^{**} - \frac{m}{r}\left[w_m^{**} - D_{2_m}^{**} + \left(-D_{3_m}^{**} + \frac{h}{2}w_{m,z}^{**} - \frac{h_s}{2}D_{1_m}^{**}\right) z_f + D_{2_m}^{**} z_f^2 + D_{3_m}^{**} z_f^2\right]\right\} T_{-m} \tag{37}$$

Constitutive Equations

The three-dimensional constitutive equations assuming linear, elastic, isotropic conditions are

$$\sigma_{r_i} = \beta\,R_i\,[\epsilon_{r_i} + \alpha_i\,(\epsilon_{z_i} + \epsilon_{\theta_i})], \qquad \tau_{rz_i} = \mu_i\,\gamma_{rz_i}, \text{ etc.} \tag{38}$$

where i denotes the material type (s or f). Where K, μ, and ν represent the bulk modulus, shear modulus, and Poisson's ratio, respectively, the material constants are

$$\beta = (3K_s + 4\mu_s/3), \qquad \alpha_i = \nu_i/(1 - \nu_i),$$

$$R_i = \begin{cases} 1, & i = s \\ (3K_f + 4\mu_f)/(3K_s + 4\mu_s), & i = f \end{cases} \tag{39}$$

Composite Strain Energy

The strain energy for a layer is ($i = s$ or f)

$$u_i = \int_{r_1}^{r_2}\frac{h_i}{2}\int_{-1}^{1}\int_0^{2\pi}\frac{1}{2}[\beta R_i(\epsilon_{r_i}^2 + \epsilon_{z_i}^2 + \epsilon_{\theta_i}^2) + 2\beta\alpha_i\,(\epsilon_{r_i}\epsilon_{\theta_i} + \epsilon_{r_i}\epsilon_{z_i} + \epsilon_{\theta_i}\epsilon_{z_i}) + \mu_i\,(\gamma_{rz_i}^2 + \gamma_{r\theta_i}^2 + \gamma_{\theta z_i}^2)]r\,d\theta\,dz_i\,dr \tag{40}$$

Inserting the strain-displacement equations into Eq. (40) and integrating with respect to θ removes its dependence and results in a sum of uncoupled integrals in r and z_i, one for each Fourier term m.[22] Further integration over the thickness of the layer removes the dependence on the intralayer coordinate z_i. The resulting expression for Fourier number m contains terms of the form

$$\int_{r_1}^{r_2} u_{m,r}^{**}\,v_m^{**}\,r\,dr, \text{ etc.} \tag{41}$$

The thickness of the layer is assumed to be small compared to the overall dimensions of the system; therefore, the variations

of the field variables and their derivatives across the thickness of the layer are small, and thus the above term is approximated as

$$\int_{r_1}^{r_2} u_{m,r}^{**}\, v_m^{**}\, r\, dr \simeq \frac{1}{h}\int_{r_1}^{r_2}\int_{-h/2}^{h/2} u_{m,r}\, v_m\, r\, dz\, dr, \text{ etc.} \quad (42)$$

The above expression assumes that the product of the two functions, evaluated at the center of the unit cell, can be approximated by the average of their product over the unit cell (the accuracy of this approximation requires that these functions be slowly varying over the unit cell). Thus, at this point, the superscripts * and ** that indicate evaluation at the center of a stiff or flexible layer have been eliminated; the resulting strain energy for a stiff layer is in the form

$$U_{s_m} = \frac{\pi}{2(1+\rho)}\int_{r_1}^{r_2}\int_{-h/2}^{h/2} \rho\, D_{s_m}\, r\, dz\, dr \quad (43)$$

where D_{s_m} contains terms of the form $u_{m,r}\, v_m$, etc. Summing over all of the stiff layers in the element (the "element" can be interpreted either as a "finite element" for the purpose of numerical analysis or a "differential element" at the global scale; A is the area of the cross section of the element, and N_s is the number of stiff layers in the element):

$$\sum_{n_s=1}^{N_s} U_{s_n} = \frac{\pi}{2(1+\rho)}\iint_A \rho\, D_{s_m}\, r\, dr\, dz \quad (44)$$

The above steps are repeated for the flexible layers. The total strain energy (for Fourier term m) for the composite system is obtained by adding the contributions for the stiff and flexible layers (the expression is given in detail by El-Hawary[25]):

$$U_m = \frac{\pi}{2(1+\rho)}\iint_A (D_{f_m} + \rho\, D_{s_m})\, r\, dr\, dz \quad (45)$$

The above expression contains no reference to the individual layers; thus, the modeling of the layered system as a homogeneous continuum is complete.

Finite-Element Analysis

The principle of minimum potential energy is used for the development of the finite-element analysis. It is assumed that the reader is familiar with general finite-element concepts; for details the reader is referred to a standard text such as Zienkiewicz.[24] Admissibility conditions require only C_0 continuity of the field variables u_m, v_m,...,δ_{θ_m} (i.e., continuity of the derivatives of the field variable is not necessary), and there are no requirements for the element unknowns D_{1_m}, D_{2_m}, D_{3_m}. Four-node isoparametric elements were used in the analysis with seven degrees of freedom (u_m, v_m,...,δ_{θ_m}) at each node and three element unknowns (D_{1_m}, D_{2_m}, D_{3_m}). In a three-dimensional analytical finite-element analysis, a two-dimensional finite-element analysis is performed for each term in the Fourier series, and the results summed to give the final solution.[19]

Rubber is a nearly incompressible material (i.e., its bulk modulus is much greater than its shear modulus), which often causes numerical difficulties for finite-element (and other numerical) procedures. Considerable work has been done to overcome this problem, either by using a mixed variational method,[26] or a penalty function or reduced integration to satisfy the constraint on the volume change in some average sense instead of pointwise.[24] Selective reduced integration was used in the current work.

After performing the global finite-element analysis, secondary dependent variables are calculated.[15] The stresses and strains for both stiff and flexible layers are calculated at the centers of the layers and at the layer interfaces by substituting the primary (field) variables into the appropriate equations [e.g., using Eqs. (7-12), (32-37), and (38)].

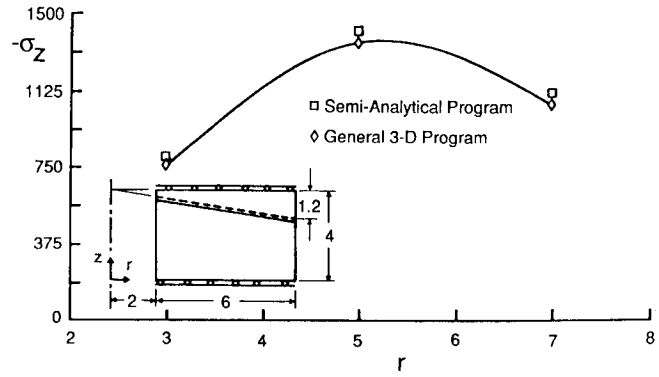

Fig. 3 σ_z vs r at $z = 3.33$ and $\theta = 15$ deg: bending problem.

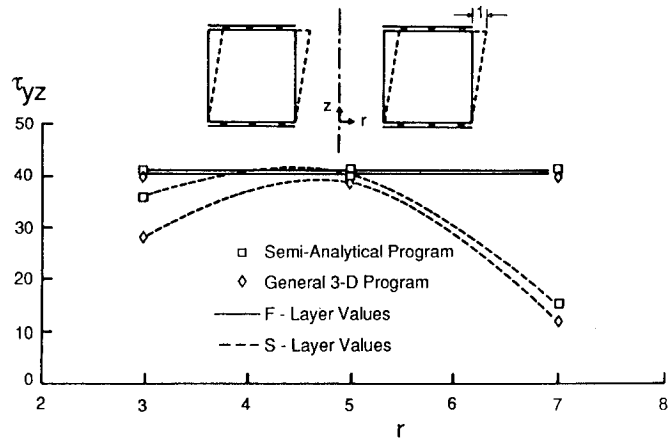

Fig. 4 τ_{yz} vs r at $\theta = 15$ deg: shear problem.

Preliminary Examples

In this section, some numerical examples are presented to illustrate the validity of the semi-analytical composite approach. For more details about problem configurations, loading conditions, and systems properties, see Ref. 25.

Bending Example

For the bending example, the specified displacement at the top surface of the bearing (see Fig. 3) is

$$w = w_0 \cos\theta \quad (46)$$

The results were checked against those given by the three-dimensional linear composite program (conventional three-dimensional, not semi-analytical) developed by Lim.[16]

For the upper layer of elements, the normal stress σ_z is plotted against r at $\theta = 15$ deg in Fig. 3 (the decision to compare results at 15 deg was based on the ease of obtaining values from the finite-element grid used by Lim). Good agreement was observed in this case.

Shear Example

The applied displacement for the shear problem is of the form $u = u_0 \cos\theta$ and $v = -u_0 \sin\theta$. The system properties and the finite-element grids for both the semi-analytical and Lim's three-dimensional analysis are the same as used in the previous bending problem. The shear stress τ_{yz} (identical for both the upper and lower layers of elements) is plotted against r for $\theta = 15$ deg for both the stiff and flexible materials using both Lim's and the current program (see Fig. 4). Good agreement is obtained between the two analyses.

Examples for Bearings Used in Helicopter Systems

In this section, comparisons are made to some of the available design formulas for elastomeric bearings for helicopter applications.

Horizontal Bearings Subjected to Torsion

The torsional stiffness of one flexible layer is considered in this section as a function of r_o for different values of r_i where r_i and r_o are the inner and outer radii of the bearing, respectively. The composite analysis is based on the assumption that both flexible and stiff layers are present and hence, strictly speaking, it is not applicable to a single flexible layer. However, the torsional flexibility is provided mainly by the flexible layers, whereas the stiff layers displace essentially as rigid bodies. Thus, for this comparison, the thickness of the steel was neglected ($h = h_f$); the validity of this approximation was tested by using different values of h_s and checking that the resulting torsional stiffness was effectively constant. A typical value for the shear modulus of rubber of 96 psi was used, and a large value (1×10^6 psi) was used for the bulk modulus to assure that Poisson's ratio would be close to 0.5. The torsional stiffness ($K_{\theta z} = M_z/\theta_z$) is defined in Eqs. (4-15) in the report by Kulkarni[3] which, rewritten in the current notations, is

$$(K_{\theta_z}/\mu_f r_o^3) = (\pi/2)(r_o/h)\{[1 - (r_i/r_o)]^4\} \tag{47}$$

The torsional stiffness predicted by the analysis was found by applying a twist of θ_z and calculating the moment of the resulting shear stress $\tau_{\theta z}$. The calculated torsional stiffnesses were compared with those given by Eq. (47) and the values given in the torsional stiffness design curves of Fig. 4-4 in Kulkarni's report.[3]

The finite-element values agree with Eq. (47) and, hence, Eqs. (4-15) of Kulkarni's report;[3] however, they don't agree with his design curves, which are partially reproduced in Fig. 5. The differences between the design curves and the equation, both reported by Kulkarni,[3] are apparently the result of an error in the design curves.

Horizontal Bearings Subjected to Bending

The variation of the bending stiffness ($K_{\theta_r} = M_r/\theta_r$) for one pad vs the bearing shape factor for different values of r_i/r_o is compared to available values. The shape factor (SF) for a rubber layer (see Ref. 16) is the ratio of the area of one loaded surface to the area free to bulge [for a circular bearing it is $(r_o - r_i)/2h_f$]. Figures 4-7 in Kulkarni's report[3] are partially reproduced in Fig. 6. Four cases were selected and checked using the current finite-element program. The bending moment is

$$M_r = \int_0^{2\pi}\int_{r_i}^{r_o} \sigma_z \cos\theta\, r^2\, dr\, d\theta \tag{48}$$

but $\sigma_z = \sigma_{z_o}\cos\theta$, where σ_{z_o} is the stress at $\theta = 0$ deg; therefore,

$$M_r = \pi\int_{r_i}^{r_o} \sigma_{z_o}\, r^2\, dr \tag{49}$$

The integration in Eq. (49) was performed numerically. The analysis was repeated for different values of Poisson's ratio, and the bending stiffness was extrapolated to $\nu = 0.5$ to obtain values corresponding to the results given by Kulkarni. Good agreement between the finite-element results and the design curves were found.

Inspecting Fig. 6, it is seen that for the same shape factor different bending stiffnesses are predicted depending on the geometry of the system. This difference is contradictory to the concept underlying the introduction of the shape factor design parameter, i.e., that bearings with the same shape factor will have similar behavior.[5] An effort was made by Ramaswamy[27] to reduce the dispersion of results by introducing a correction term to the usual definition of shape factor, i.e., $SF_b = CF \times SF$, where SF_b is the corrected shape factor, and the correction factor (CF) is given by Ramaswamy[27] as

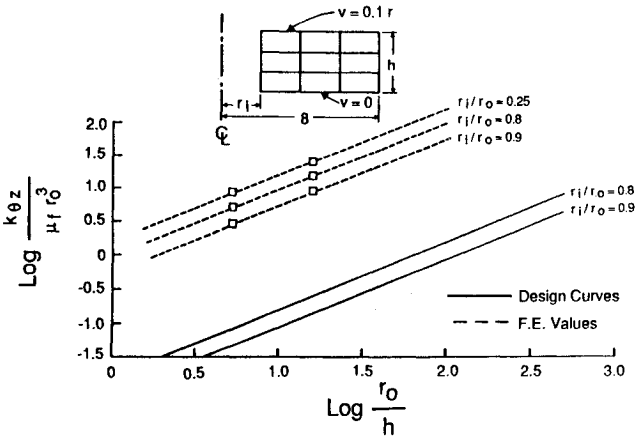

Fig. 5 Torsional stiffness: design curves.

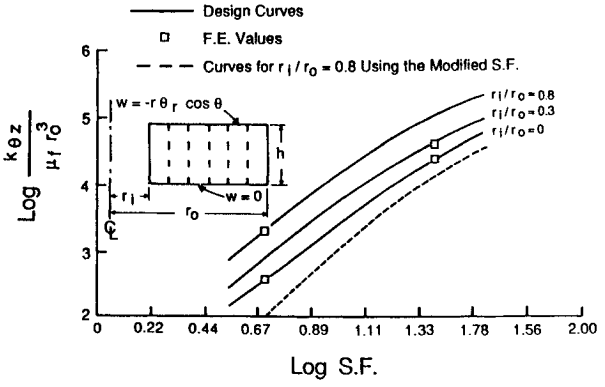

Fig. 6 Bending stiffness vs shape factor: design curves.

$$CF = [\tfrac{1}{2}\,(R_p/R)^2]^{-1.45} \tag{50}$$

where R and R_p are the radii of gyration, about the bending axis, of the loaded area and the area of the perimeter (area free to bulge), respectively. For a circular bearing

$$R^2 = (r_o^2 + r_i^2)/4 \tag{51a}$$

$$R_p^2 = \tfrac{1}{2}\,(r_o^3 + r_i^3)/(r_o + r_i) \tag{51b}$$

The correction factor is 1 for $r_i/r_o = 0$, which means that the curve for $r_i/r_o = 0$ in Fig. 6 will not change. The curve for $r_i/r_o = 0.8$, however, does change; it is redrawn in the figure after correction. The difference between the two corrected curves is much smaller than before; however, the correction factor still needs some refinement before the difference is completely eliminated.

Parameter Study

This parameter study was performed in order to illustrate the versatility and usefulness of the analysis in generating design information for proposed novel bearing designs. Horizontally layered circular bearings with conical central openings were selected for the parameter study (see Fig. 7). The parameter investigated in the study is the angle Ψ between the inner surface of the bearing and the vertical z axis. The reference bearing $\Psi = 0$ is shown in Fig. 7a and the finite-ele-

ment grid for a typical bearing in Fig. 7b. The effects of Ψ on the compressive, bending, torsional, and shear stiffnesses are investigated in the subsequent sections. The range of Ψ is varied between 0 and 72 deg, and the system properties are $H = 3$ in., $h_s = 0.3$ in., $h_f = 0.3$ in., $\mu_f = 110$ psi, $K_f = 5500$ psi, $E_s = 3 \times 10^7$ psi, and $\nu_s = 0.3$. The shape factor for the reference bearing was chosen to be 10.

Compressive Stiffness

The upper surface of each bearing was uniformly displaced by the amount δ, and the compressive force F_z was calulated by integrating σ_z over the loaded area. Unlike the compression example in the previous section, for nonzero values of Ψ the stress σ_z is not constant in the z direction, and so the values of stress were linearly extrapolated from the element centers to the upper surface. The compressive stiffness is reported in terms of the dimensionless quantity $(F_z/3\ \mu_f\ \pi\ H^2)/(\delta/H/2)$. The effect of the angle Ψ on the compressive stiffness is shown in Fig. 8; it is almost negligible up to 30 deg. At $\Psi = 72$ deg the compressive stiffness is about 30% of that of the reference system $\Psi = 0$.

Bending Stiffness

The bending moment due to an applied rotation of the upper surface is given by Eq. (49). Extrapolating values of σ_z to the upper surface, the bending moment M_r was calculated by numerical integration. The bending stiffness is expressed in terms of the dimensionless quantity $M_r/[(\theta_r/H)\mu_f(r_o^4 - r_i^4)]$ where r_o and r_i are the outer and inner radii of the reference system, respectively. The effect of Ψ on the bending stiffness is shown in Fig. 9.

Torsional Stiffness

The torque M_z due to an applied twist θ_z is found by numerically integrating the moment produced by $\tau_{\theta z}$ (extrapolating the stress to the upper surface). The torsional stiffness is expressed in terms of the dimensionless quantity $M_z/[(\theta_z/H)\ \mu_f(r_o^4 - r_i^4)]$. The variation of the torsional stiffness vs Ψ is shown in Fig. 10. One of the important characteristics of an elastomeric bearing, that it is much more flexible in torsion than bending, is illustrated by these results, i.e., the torsional stiffness is about 5% of the bending stiffness.

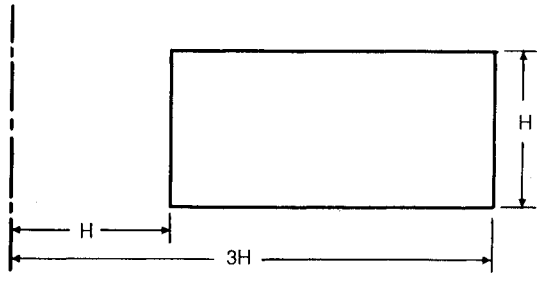

a) Reference system

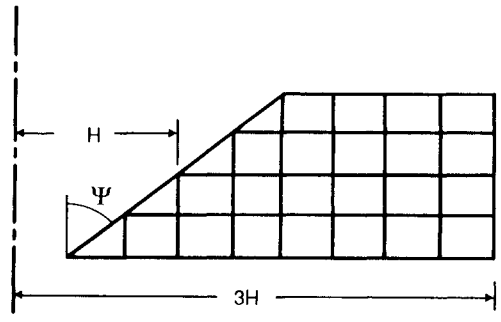

b) Finite-element grid

Fig. 7 Parameter study.

Shear Stiffness

The shear force V due to an applied shear displacement is found by numerically integrating the shear stress τ_{xz}. The shear stiffness is expressed in terms of the dimensionless quantity $[V/3\mu_f\pi H^2]/[\delta_s/H/2]$. The variation of the shear stiffness vs Ψ is shown in Fig. 11.

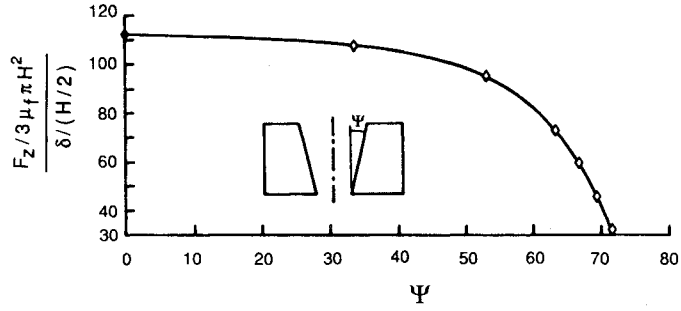

Fig. 8 Effect of angle Ψ on compressive stiffness.

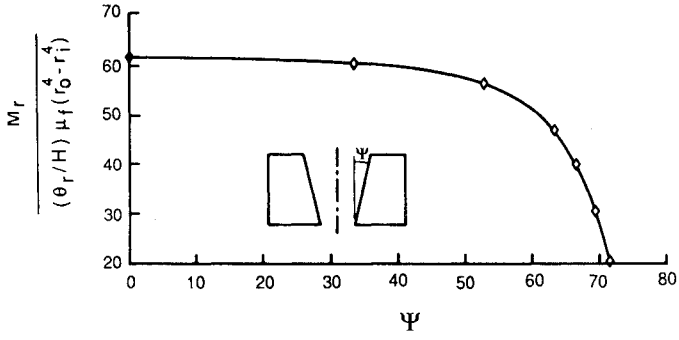

Fig. 9 Effect of angle Ψ on bending stiffness.

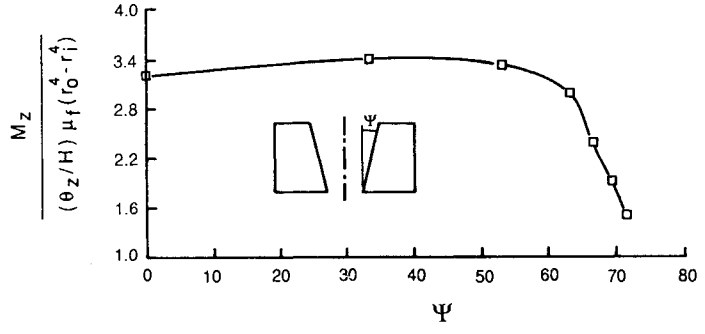

Fig. 10 Effect of angle Ψ on torsional stiffness.

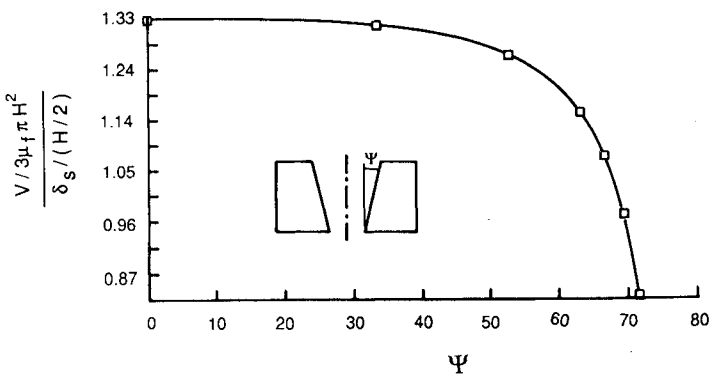

Fig. 11 Effect of angle Ψ on shear stiffness.

The important characteristic of an elastomeric bearing, that it is flexible in shear and stiff in compression, is illustrated in this example, as the shear stiffness is about 1.2% of the compressive stiffness.

Conclusions

A linear three-dimensional, equivalent homogeneous, composite theory, and accompanying finite-element analysis for elastomeric bearings of revolution with horizonal layers and nonaxisymmetric loads, have been developed. The theory is limited to linear materials and small displacements and deformations. The theory, however, has been so developed that in the future it can be extended to include material and geometric nonlinearities. This extension would be similar to that performed for rectangular bearings by Herrmann, Shafigh-Nobari, and Hamidi.[28]

The composite theory is computationally very economical and thus would appear to offer many advantages over a discrete analysis. In addition, the use of the semianalytical finite-element procedure furnishes additional savings by expressing the three-dimensional analysis in terms of a series of two-dimensional ones.

Some of the design procedures used for elastomeric bearings for helicopter systems were checked. Good agreement between the design curves and the finite-element analysis was found, except for one case where an error is suspected to exist in the design curves.

As an illustration of the generality of the composite theory and analysis, the behavior of a circular bearing with a conical central hole was studied. The angle defining the conical surface was considered as a design parameter. Its effect was found to be negligible up to about 30 deg after which the bearing stiffness tends to fall off rapidly.

The current theory may be expanded to include axisymmetric bearings with nonhorizontal layers by extending the semianalytical concept to the general configurations considered by El-Hawary[18] for axisymmetric loading.

References

[1]Derham, C. J. and Thomas, A. G., "The Design and Use of Rubber Bearings for Vibration Isolation and Seismic Protection of Structures," *Engineering Structures*, Vol. 2, No. 3, July 1980, pp. 171–175.

[2]"Development of an Elastomeric Seal for Omniaxial Movable Nozzles (lockseal)," Lockhead Propulsion Co., Palo Alto, CA, TR AFRPL-TR-66-112, 1966.

[3]Kulkarni, S. B., "Design Criteria for Elastomeric Bearings, Volume II Design Manual," Thiokal/Wasatch Div., Brigham City, UT, AD/A-024767, 1976.

[4]Clark, E. V. and Moultrop, K., "Load – Deformation Characteristics of Elastomeric Bridge Bearing Pads," *Highway Research Record*, Vol. 34, 1963, pp. 90–116.

[5]Stanton, J. F. and Roeder, C. W., "Elastomeric Bearings Design, Construction and Materials," Transportation Research Board, National Research Council, Washington, DC, National Cooperative Highway Research Program Rept. 248, 1982.

[6]Soni, M. L., "A Microstructure Continuum Theory for Laminated Elastic Composites," Ph.D Dissertation, Univ. of Texas, Austin, TX, 1977.

[7]Hermann, L. R., "Finite Element Modeling of Composite Edge Effects," *ASCE, 7th Conf. on Electronic Computations*, American Society of Civil Engineers, New York, 1979, pp. 593–607.

[8]Herrmann, L. R. and Schamber, R. A., "Finite Element Analysis of Layered Systems with Edge Effects," *Numerical Methods for Coupled Problems*, Pineridge Press, Swansea, UK, 1981, pp 418–429.

[9]Moore, J. K. and Herrmann, L. R., "A Stress-Strain Analysis of Rubber and Steel Composite Bearings," *Proceedings of the 4th Engineering Mechanics Div. Specialty Conf. on Recent Advances in Engineering Mechanics and Their Impact on Civil Engineering Practice, ASCE*, Vol. 2, Purdue Univ., West Lafayette, IN, 1983, pp. 734–737.

[10]Herrmann, L. R., "Effects of Edge Conditions on Test Results for Concrete," *Cement and Concrete Research*, Vol. 8, Jan. 1978, pp. 25–36.

[11]Wang, A. S. D. and Crossman, F. W., "Calculation of Edge Effects in Multi-Layer Laminates by Substructuring," *Journal of Composite Materials*, Vol. 12, Jan. 1978, pp. 76–83.

[12]Sun, C. T., Achenback, J. D., and Hermann, G., "Continuum Theory for a Laminated Medium," *J.A.M.*, Vol. 35, Sept. 1968, pp. 467–475.

[13]Eringen, A. C., "Linear Theory of Micropolar Elasticity," *Journal of Mathematics and Mechanics*, Vol. 15, June 1966, pp. 909–923.

[14]Hermann, L. R., "Mixed Finite Elements for Couple-Stress Analysis," *Hybrid and Mixed Finite Element Methods*, edited by S. N. Atluri, R. H. Gallagher, and O. C. Zienkiewicz, Wiley, Chichester, England, 1983, pp. 1–18.

[15]Herrmann, L. R., Welch, K. R., and Lim, C. K., "Composite FEM Analysis for Layered Systems," *ASCE Journal of Engineering Mechanics*, Vol. 110, Sept. 1984, pp. 1284–1302.

[16]Lim, C. K. and Herrmann, L. R., "Equivalent Homogeneous F.E. Model for Elastomeric Bearings," *ASCE Journal of Engineering Mechanics*, Vol. 113, Jan. 1987, pp. 106–125.

[17]Hamidi, R., "A Three-Dimensional Nonlinear Composite Finite Element Analysis of Elastomeric Bridge Bearings," M.S. Thesis, Dept. of Civil Engineering, Univ. of California, Davis, Davis, CA, 1986.

[18]El-Hawary, M. and Herrmann, L. R., "An Axisymmetric Finite Element Study for Elastomeric Composites," *ASCE Journal of Eingineering Mechanics*, Vol. 114, Aug. 1988, pp. 1355–1374.

[19]Herrmann, L. R., "Three-DImensional Elasticity Analysis of Non-Axisymmetrically Loaded Solids of Revolution," Dept. of Civil Engineering, Rept. No. 68-21-1, Univ. of California, Davis, Davis, CA, 1968.

[20]Pardoen, G. C., Falco, A. D., and Crose, J. G., "Axisymmetric Stress Analysis of Axisymmetric Solids with Rectangularly Orthotropic Properties," *AIAA Journal*, Vol. 14, Oct. 1976, 1419–1426.

[21]Cheung, Y. K., *Finite Strip Method in Structural Analysis*, Pergamon Press, New York, 1976.

[22]Sedaghat, M., Herrmann, L. R., "A Nonlinear, Semi-Analytical Finite Element Analysis of Nearly Axisymmetric Solids," *Journal of Computers and Structures*, Vol. 17, No. 3, 1983, pp. 389–401.

[23]Nayfeh, A. H., *Pertubation Methods*, Wiley, New York, 1973.

[24]Zienkiewicz, O. C., *The Finite Element Method in Engineering and Science*, 3rd ed., McGraw-Hill, London, 1977.

[25]El-Hawary, M. M., "A Finite Element Study for Elastomeric Composite Solids of Revolution," Ph.D. Thesis, Dept. of Civil Engineering, Univ. of California, Davis, CA, 1987.

[26]Moore, J. K., "A Nonlinear Finite Element Analysis of Elastomeric Bearings," Ph.D Thesis, Dept. of Civil Engineering, Univ. of California, Davis, Davis, CA, 1982.

[27]Ramaswamy, A., "Applications of 2-D Composite Finite Element Analysis to Elastomeric Bearing Problems," M.S. Thesis, Dept. of Civil Engineering, Univ. of California, Davis, Davis, CA, 1986.

[28]Herrmann, L. R., Shafigh-Nobari, F., and Hamidi, R., "On the Verification of a Finite Element Analysis for Elastomeric Bridge Bearings," *2nd World Congress on Joints, Sealings and Bearings Systems for Concrete Structures*, American Concrete Institute, Detroit, MI, 1986, pp. 1–30.